SORBONNE UNIVERSITÉ

MATHÉMATIQUES DE LA MODÉLISATION

Numerical Analysis of blood flow in a bifurcation and of explicit schemes for FSI

Project Report

of

MODÈLES MATHÉMATIQUES ET MÉTHODES NUMÉRIQUES POUR LA SIMULATION EN HÉMODYNAMIQUE

Renee Crispo

March 21, 2025

Abstract

This work explores the numerical modeling of blood flow in an arterial bifurcation and fluid-structure interaction (FSI) in an elastic tube. In the first part, we address the discretization of the Navier-Stokes equations for incompressible fluids, with particular focus on the strong and variational formulations, conditional stability in the energy norm, and numerical implementation using FreeFem++. In the second part, we analyze numerical instabilities arising from explicit schemes for FSI, comparing explicit Dirichlet and explicit Robin coupling conditions. The results show that the Robin scheme ensures robustness regardless of the added-mass effect, while the Dirichlet scheme can be unstable.

Contents

1   Simulation of Blood Flow in a Bifurcation

The first part of the project aims to model blood flow in a simplified bi-dimensional bifurcation, shown in Figure 1. Given $T > 0$, the goal is to solve Navier-Stokes equations for incompressible flows: we look for the velocity $\mathbf{u} : \Omega \times (0, T) \to \mathbb{R}^2$ and the pressure $p : \Omega \times (0, T) \to \mathbb{R}$ that solve

$$\begin{cases} \rho^{\mathrm{f}} \left(\dfrac{\partial \mathbf{u}}{\partial t} + \mathbf{u} \cdot \nabla \mathbf{u} \right) - \nabla \cdot \boldsymbol{\sigma}(\mathbf{u}, p) = \mathbf{0}, & \text{in } \Omega \times (0, T), \\ \nabla \cdot \mathbf{u} = 0, & \text{in } \Omega \times (0, T). \end{cases} \tag{1}$$

where

$$\boldsymbol{\sigma}(\mathbf{u}, p) := 2\mu\varepsilon(\mathbf{u}) - p\mathbf{I}, \quad \varepsilon(\mathbf{u}) := \frac{1}{2} \left(\nabla \mathbf{u} + (\nabla \mathbf{u})^T \right). \tag{2}$$

The Cauchy stress tensor $\boldsymbol{\sigma}(\mathbf{u}, p)$ describes the internal forces per unit area within a fluid due to pressure and viscosity μ. It is related to the strain rate tensor $\varepsilon(\mathbf{u})$, which is the symmetric part of the gradient of the velocity, measuring the local deformation rate of the fluid.
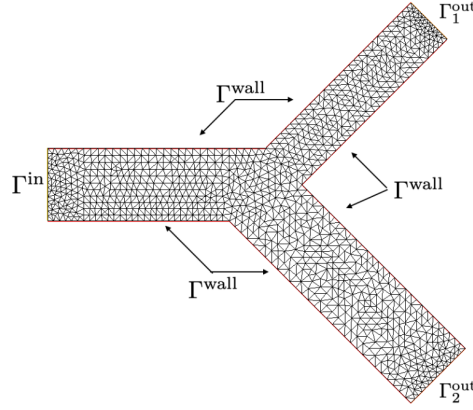

Figure 1: *Computational domain* Ω

1.1   Physical meaning of the boundary conditions

In order to solve (1), the imposed boundary conditions are

$$\begin{cases} \mathbf{u} = \mathbf{0} & \text{on } \Gamma^{\mathrm{wall}} \times (0, T) \\ \mathbf{u} = \mathbf{u}_{\mathrm{in}} & \text{on } \Gamma^{\mathrm{in}} \times (0, T) \\ \boldsymbol{\sigma}(\mathbf{u}, p)\mathbf{n} - \dfrac{\rho^{\mathrm{f}}}{2} |\mathbf{u} \cdot \mathbf{n}|_{-} \mathbf{u} = -p_{\mathrm{out},1}\mathbf{n} & \text{on } \Gamma_1^{\mathrm{out}} \times (0, T) \\ \boldsymbol{\sigma}(\mathbf{u}, p)\mathbf{n} - \dfrac{\rho^{\mathrm{f}}}{2} |\mathbf{u} \cdot \mathbf{n}|_{-} \mathbf{u} = -p_{\mathrm{out},2}\mathbf{n} & \text{on } \Gamma_2^{\mathrm{out}} \times (0, T) \end{cases} \tag{3}$$

where $\mathbf{n}$ is the outward normal unit vector and $|x|_{-} = \min\{x, 0\}$.

The first equation, $\mathbf{u} = \mathbf{0}$, represents a no-slip condition. This means that if the wall is stationary, the fluid particles in direct contact with it have zero velocity relative to the wall, preventing any slippage. In practice, it ensures that blood does not slip against vessel walls. This is a very simplified representation of the flow, indeed in reality, the vessel walls are elastic

and governed by an additional set of equations controlling their deformation.

The constraint imposed at the inlet is a Dirichlet boundary condition that forces the velocity to be equal to

$$\mathbf{u}_{\text{in}} = \begin{pmatrix} \tilde{g}(t)(0.4 - y)y \\ 0 \end{pmatrix}$$

where $\tilde{g} : [0, T] \to \mathbb{R}$ is obtained as the periodic extension of the function

$$g(t) = \begin{cases} 1000 \sin(\pi t/0.4) & \text{if } t \in [0, 0.4] \\ 0 & \text{if } (0.4, 0.8] \end{cases}$$

This condition forces the velocity to have a parabolic profile with the flow reaching the highest velocity in the center of the channel and a null velocity at the walls. The function $\tilde{g}$ is periodic so that it captures the nature of heart's pumps. One pump is formed of two different phases: the systolic phase, when blood is actively pumped into the system, and the diastolic phase, which is a rest phase.

Lastly, the outward conditions on the two outlet boundaries, Γ_1^{out} and Γ_2^{out}, represent a model where the pressure depends on the resistance in downstream vasculature:

$$p_{\text{out},i} = p_d + R_{d,i} \int_{\Gamma_i^{\text{out}}} \mathbf{u} \cdot \mathbf{n} \qquad i = 1, 2$$

From a mathematical point of view, these conditions are referred to as *backward stabilization*: they are a specific case of a more general formula stated in [1]. These conditions were proposed in [2] in order to reduce the outlet instabilities. Practically speaking, they accounts for how real arteries interact with the rest of the circulatory system, where resistance from smaller arteries and capillaries determines the flow rate.

1.2 Discretization of the problem: strong and variational formulation

Given a time interval Δt, let us define $t^n = n\Delta t, n \in \mathbb{N}$, as well as the approximation in time of the velocity $\mathbf{u}^n \simeq \mathbf{u}(t_n)$ and of the pressure $p^n \simeq p(t_n)$. Therefore, we approximate the time derivative as

$$\frac{\partial \mathbf{u}^n}{\partial t} = \frac{\mathbf{u}^n - \mathbf{u}^{n-1}}{\Delta t}$$

The strong formulation reads:

Given $\mathbf{u}_0 = \mathbf{u}(0)$, find $\forall n \geq 1$ $(\mathbf{u}^n, p^n)$ such that

$$\begin{cases} \rho^f \left(\dfrac{\mathbf{u}^n - \mathbf{u}^{n-1}}{\Delta t} + \mathbf{u}^{n-1} \cdot \nabla \mathbf{u}^n \right) - \nabla \cdot \boldsymbol{\sigma}(\mathbf{u}^n, p^n) = \mathbf{0} & \text{in } \Omega \\ \nabla \cdot \mathbf{u}^n = 0 & \text{in } \Omega \\ \mathbf{u}^n = \mathbf{0} & \text{on } \Gamma^{\text{wall}} \\ \mathbf{u}^n = \mathbf{u}_{\text{in}}^n & \text{on } \Gamma^{\text{in}} \\ \boldsymbol{\sigma}(\mathbf{u}^n, p^n)\mathbf{n} - \dfrac{\rho^f}{2}|\mathbf{u}^{n-1} \cdot \mathbf{n}|_- \mathbf{u}^n = -p_{\text{out},1}^n \mathbf{n} & \text{on } \Gamma_1^{\text{out}} \\ \boldsymbol{\sigma}(\mathbf{u}^n, p^n)\mathbf{n} - \dfrac{\rho^f}{2}|\mathbf{u}^{n-1} \cdot \mathbf{n}|_- \mathbf{u}^n = -p_{\text{out},2}^n \mathbf{n} & \text{on } \Gamma_2^{\text{out}} \end{cases} \qquad (4)$$

where $(4)_{3,4}$ are being treated explicitly, i.e.

$$p_{\text{out},i}^n = p_d + R_{d,i} \int_{\Gamma_i^{\text{out}}} \mathbf{u}^{n-1} \cdot \mathbf{n} \qquad i = 1,2$$

We have used a semi-implicit scheme: indeed, the non-linear convective term $\mathbf{u} \cdot \nabla \mathbf{u}$ is evaluated as $\mathbf{u}^{n-1} \cdot \nabla \mathbf{u}^n$. As a consequence, to maintain coherence, the same approach is used for the non linear term in the outlet boundary conditions. This approach will come in handy later for in proving the numerical stability in the energy norm.

Then, consider two general test functions $\mathbf{v}$ and q of enough regularity. Multiply the momentum equation $(4)_1$ by $\mathbf{v}$ and the incompressibility condition $(4)_2$ by q. Then, after integrating over the whole domain Ω, we can obtain the mixed variational formulation:

$$\begin{cases} \int_\Omega \rho^{\text{f}} \left(\dfrac{\mathbf{u}^n - \mathbf{u}^{n-1}}{\Delta t} + \mathbf{u}^{n-1} \cdot \nabla \mathbf{u}^n \right) \mathbf{v} - \int_\Omega \nabla \cdot \boldsymbol{\sigma}(\mathbf{u}^n, p^n) \mathbf{v} = 0 \\ \int_\Omega \nabla \cdot \mathbf{u}^n q = 0 \end{cases}$$

The momentum equation can be rewritten as

$$\int_\Omega \rho^{\text{f}} \frac{\mathbf{u}^n - \mathbf{u}^{n-1}}{\Delta t} \mathbf{v} + \int_\Omega \rho^{\text{f}} \mathbf{u}^{n-1} \cdot \nabla \mathbf{u}^n \, \mathbf{v} - \underbrace{\int_{\partial \Omega} \boldsymbol{\sigma}(\mathbf{u}^n, p^n) \mathbf{n} \cdot \mathbf{v}}_{(a)} + \underbrace{\int_\Omega \boldsymbol{\sigma}(\mathbf{u}^n, p^n) : \nabla \mathbf{v}}_{(b)} = 0$$

Let us concentrate separately on the two terms:

(a) We choose a specific set of test functions such that $\mathbf{v} = \mathbf{0}$ on $\Gamma^{\text{wall}} \cup \Gamma^{\text{in}}$. In such a way, the terms on $\Gamma^{\text{wall}} \cup \Gamma^{\text{in}}$ are null and this integral can be rewritten as

$$\int_{\partial \Omega} \boldsymbol{\sigma}(\mathbf{u}^n, p^n) \mathbf{v} \cdot \mathbf{n} = \int_{\Gamma_1^{\text{out}}} \boldsymbol{\sigma}(\mathbf{u}^n, p^n) \mathbf{v} \cdot \mathbf{n} + \int_{\Gamma_2^{\text{out}}} \boldsymbol{\sigma}(\mathbf{u}^n, p^n) \mathbf{v} \cdot \mathbf{n}$$

$$= \int_{\Gamma_1^{\text{out}}} \left(\frac{\rho^{\text{f}}}{2} |\mathbf{u}^{n-1} \cdot \mathbf{n}|_- \mathbf{u}^n - p_{\text{out},1}^n \right) \mathbf{n} \cdot \mathbf{v} + \int_{\Gamma_2^{\text{out}}} \left(\frac{\rho^{\text{f}}}{2} |\mathbf{u}^{n-1} \cdot \mathbf{n}|_- \mathbf{u}^n - p_{\text{out},2}^n \right) \mathbf{n} \cdot \mathbf{v}$$

(b) To simplify this term, recall the definition of the stresses $\boldsymbol{\sigma}(\mathbf{u}^n, p^n)$:

$$\boldsymbol{\sigma}(\mathbf{u}^n, p^n) := 2\mu\varepsilon(\mathbf{u}^n) - p^n \mathbf{I}$$

Using the property that $\mathbf{I} : \nabla \mathbf{v} = \text{tr}(\mathbf{v}) = \nabla \cdot \mathbf{v}$ and considering only the symmetric part of $\nabla \mathbf{u}$, the term becomes

$$\int_\Omega (2\mu\varepsilon(\mathbf{u}^n) - p^n \mathbf{I}) : \nabla \mathbf{v} = \int_\Omega 2\mu\varepsilon(\mathbf{u}^n) : \nabla \mathbf{v} - \int_\Omega p \nabla \cdot \mathbf{v} = \int_\Omega 2\mu\varepsilon(\mathbf{u}^n) : \varepsilon(\mathbf{v}) - \int_\Omega p \nabla \cdot \mathbf{v}$$

As a consequence, the candidate spaces for the test functions $\mathbf{v}$ and q are respectively

$$X = H_{\Gamma^{\text{in}} \cup \Gamma^{\text{wall}}}^1 = \{ \mathbf{v} \in H^1(\Omega) : \mathbf{v} = \mathbf{0} \text{ on } \Gamma^{\text{in}} \cup \Gamma^{\text{wall}} \}, \qquad M = L^2$$

The candidate space for the solution is

$$X^{\text{in}} = \{\mathbf{v} \in H^1(\Omega) : \mathbf{v} = \mathbf{u}_{\text{in}} \text{ on } \Gamma^{\text{in}}, \mathbf{v} = \mathbf{0} \text{ on } \Gamma^{\text{wall}}\}$$

Moreover, in order to lighten the notation, we define the following functionals:

$$a(\mathbf{u}^n, \mathbf{u}^{n-1}, \mathbf{v}) := \int_\Omega \rho^{\text{f}} \frac{\mathbf{u}^n - \mathbf{u}^{n-1}}{\Delta t} \mathbf{v} + \int_\Omega \rho^{\text{f}} \mathbf{u}^{n-1} \cdot \nabla \mathbf{u}^n \, \mathbf{v} + \int_\Omega 2\mu\varepsilon(\mathbf{u}^n) : \varepsilon(\mathbf{v})$$

$$b(\mathbf{v}, p^n) := -\int_\Omega \nabla \cdot \mathbf{v} \, p^n$$

$$l(\mathbf{u}^n, \mathbf{u}^{n-1}, \mathbf{v}) := \sum_{i=1}^{2} \int_{\Gamma_i^{\text{out}}} \left(\frac{\rho^{\text{f}}}{2} |\mathbf{u}^{n-1} \cdot \mathbf{n}|_- \mathbf{u}^n - p_{\text{out,i}}^n \right) \mathbf{n} \cdot \mathbf{v}$$

The resulting formulation is

Find $(\mathbf{u}^n, p^n) \in X^{\text{in}} \times M$ such that $\forall \mathbf{v} \in X$

$$\begin{cases} a(\mathbf{u}^n, \mathbf{u}^{n-1}, \mathbf{v}) + b(\mathbf{v}, p^n) = l(\mathbf{u}^n, \mathbf{u}^{n-1}, \mathbf{v}) & \forall \mathbf{v} \in X \\ b(\mathbf{u}^n, q) = 0 & \forall q \in M \end{cases} \tag{5}$$

Formulation (5) is problematic since the space X^{in} is not a vector space, but rather an affine space. This prevents us from proving coercivity of the trilinear form $a(\mathbf{u}^n, \mathbf{u}^{n-1}, \mathbf{v})$ since we would not be able to take $\mathbf{u} = \mathbf{v}$. To resolve this, the lifting operator $\mathcal{L}_{\text{in}} : H^{1/2}(\partial\Omega) \to H^1(\Omega)$ is introduced. This operator is defined such that

$$\mathcal{L}_{\text{in}}|_{\Gamma^{\text{in}} \cup \Gamma^{\text{wall}}} = \begin{cases} \mathbf{u}_{\text{in}} & \text{on } \Gamma^{\text{in}} \\ \mathbf{0} & \text{on } \Gamma^{\text{wall}} \end{cases}$$

Therefore, the solution can be decomposed as the sum of two pieces

$$\mathbf{u} = \mathbf{w} + \mathcal{L}_{\text{in}}$$

Clearly, $\mathbf{w} \in X$, i.e. it has homogeneous boundary condition at the inlet and on the walls, and $\nabla\mathbf{w} = \nabla\mathbf{u} - \nabla\mathcal{L}_{\text{in}}$. The final mixed variational formulation becomes:

Find $(\mathbf{w}^n, p^n) \in X \times M$ such that $\forall \mathbf{v} \in X$

$$\begin{cases} a(\mathbf{w}^n, \mathbf{u}^{n-1}, \mathbf{v}) + b(\mathbf{v}, p^n) = l(\mathbf{u}^n, \mathbf{u}^{n-1}, \mathbf{v}) - a(\mathcal{L}_{\text{in}}^n, \mathbf{u}^{n-1}, \mathbf{v}) \\ b(\mathbf{w}^n, q) = 0 \end{cases}$$

since $b(\mathcal{L}_{\text{in}}^n, q) = \int_\Omega \nabla \cdot \mathcal{L}_{\text{in}}^n q = 0$, being the lifting operator divergence free.

1.3 Fully discrete formulation and examples of FE spaces

Let us introduce a finite element triangulation $\mathcal{T}_h$ of Ω. Define the discrete spaces $X_h \subset X$, $X_h^{\text{in}} \subset X^{\text{in}}$ and $M_h \subset M$, such that $\dim X_h < +\infty$, $\dim X_h^{\text{in}} < +\infty$ and $\dim M_h < +\infty$. The fully

discrete axisymmetric problem reads:

Find $(\mathbf{u}_h^n, p_h^n) \in X_h^{\mathrm{in}} \times M_h$ such that $\forall \mathbf{v}_h \in X_h$

$$
\begin{cases}
a(\mathbf{u}_h^n, \mathbf{u}_h^{n-1}, \mathbf{v}_h) + b(\mathbf{v}_h, p_h^n) = l(\mathbf{u}_h^n, \mathbf{u}_h^{n-1}, \mathbf{v}_h) & \forall \mathbf{v}_h \in X \\
b(\mathbf{u}_h^n, q_h) = 0 & \forall q_h \in M
\end{cases}
\tag{6}
$$

On the other hand, the symmetric formulation with the lifting operator is

Find $(\mathbf{w}_h^{\,n}, p_h^n) \in X_h \times M_h$ such that $\forall \mathbf{v}_h \in X_h$

$$
\begin{cases}
a(\mathbf{w}_h^n, \mathbf{u}_h^{n-1}, \mathbf{v}_h) + b(\mathbf{v}_h, p_h^n) = l(\mathbf{u}_h^n, \mathbf{u}_h^{n-1}, \mathbf{v}_h) - a(\mathcal{L}_{\mathrm{in},h}^n, \mathbf{u}_h^{n-1}, \mathbf{v}_h) \\
b(\mathbf{w}_h^n, q_h) = 0
\end{cases}
$$

The choice of the discrete spaces X_h and M_h is fundamental to ensuring the well-posedness of the problem and guaranteeing the satisfaction of the discrete inf-sup condition:

$$
\exists \beta_h > 0 \quad \text{such that} \quad \inf_{q_h \in M_h \setminus \{0\}} \sup_{\mathbf{v}_h \in X_h \setminus \{\mathbf{0}\}} \frac{|b(\mathbf{v}_h, q_h)|}{\|\mathbf{v}_h\| \, \|q_h\|} \geq \beta
$$

Indeed, this condition is not automatically inherited from the continuous formulation. Some appropriate choices [3], also illustrated in Figure 2, are:

- Taylor-Hood elements: $\mathbb{P}^k - \mathbb{P}^{k-1}, \forall k \geq 2$. The smallest pair of spaces is represented by $\mathbb{P}^2 - \mathbb{P}^1$ where the velocity is approximated using piecewise quadratic continuous polynomials, while the pressure is represented by piecewise linear continuous polynomials.

- $\mathbb{P}^k - \mathbb{P}_D^{k-2}, k \geq 2$. This family uses continuous polynomials of degree k for the velocity and discontinuous polynomials of degree $k - 2$ for the pressure. For instance, choosing $k = 3$ gives $\mathbb{P}^3 - \mathbb{P}_D^1$, where the velocity space consists of piecewise cubic continuous polynomials, while the pressure space consists of piecewise linear discontinuous polynomials.

- $iso\mathbb{P}^2 - \mathbb{P}^1$. Both velocity and pressure are approximated using piecewise continuous linear polynomials, but the velocity is computed on a twice as fine mesh.

1.4   Conditional stability in the energy norm

For this section only, additionally suppose that $\mathbf{u}_{\mathrm{in}} = \mathbf{0}$ on $\Gamma^{\mathrm{in}} \times (0, T)$. Therefore, we can work with (6), with no need to introduce the lifting operator.

Lemma 1.1. (**Conditional energy stability**) *Problem* (6) *is stable in the energy norm under the condition*

$$
\Delta t \leq \frac{\rho^{\mathrm{f}} h}{C_T \sum_{i=1}^2 R_{d,i} |\Gamma_i^{\mathrm{out}}|}
$$

Proof. In formulation $(6)_1$ choose $\mathbf{v}_h = \mathbf{u}_h^n$ and integrate over the whole domain Ω:

$$
\int_\Omega \left[\rho^{\mathrm{f}} \left(\frac{\mathbf{u}_h^n - \mathbf{u}_h^{n-1}}{\Delta t} \mathbf{u}_h^n + \mathbf{u}_h^{n-1} \cdot \nabla \mathbf{u}_h^n \mathbf{u}_h^n \right) - \nabla \cdot \boldsymbol{\sigma}(\mathbf{u}_h^n, p_h^n) \mathbf{u}_h^n \right] = 0
\tag{7}
$$

(a) *Taylor-Hood, k = 2*

(b) $\mathbb{P}^k - \mathbb{P}_D^{k-2}, k = 2$:
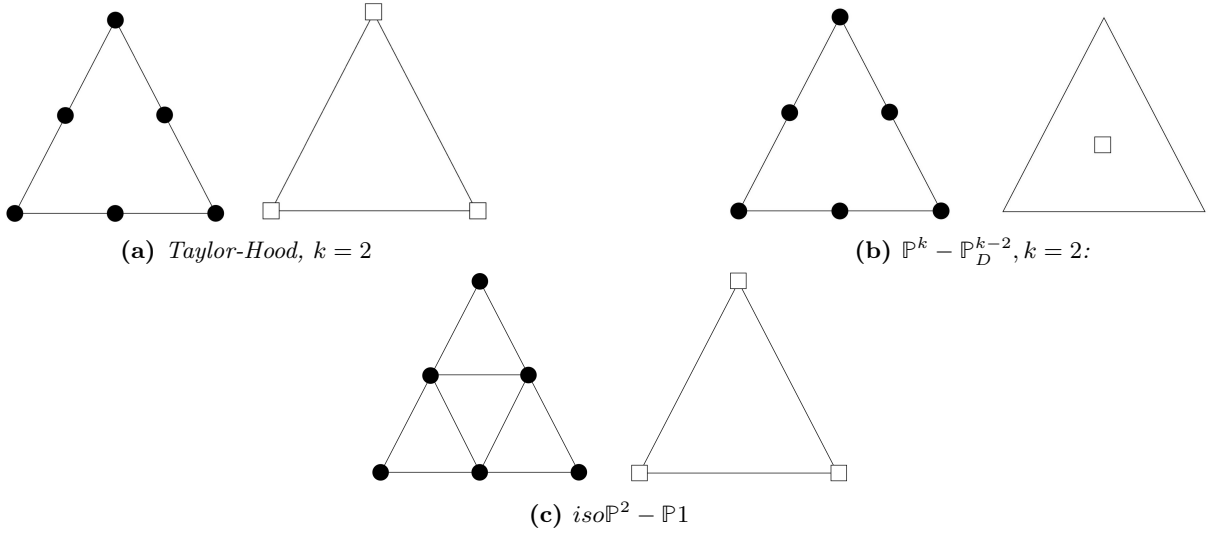
(c) $iso\mathbb{P}^2 - \mathbb{P}1$

Figure 2: *FE spaces that satisfy the discrete inf-sup condition. The symbol ● identifies the degrees of freedom of the velocity and □ indicates the ones of the pressure.*

Let us consider each term of (7) separately. Using the identity $(a - b)a = \frac{1}{2}[a^2 - b^2 + (a - b)^2]$, the first term can be rewritten as:

$$\rho^{\mathrm{f}} \int_\Omega \frac{\mathbf{u}_h^n - \mathbf{u}_h^{n-1}}{\Delta t} \mathbf{u}_h^n = \frac{\rho^{\mathrm{f}}}{2\Delta t} \left[\|\mathbf{u}_h^n\|_{L^2(\Omega)}^2 - \|\mathbf{u}_h^{n-1}\|_{L^2(\Omega)}^2 + \|\mathbf{u}_h^n - \mathbf{u}_h^{n-1}\|_{L^2(\Omega)}^2 \right]$$

The second term can simplified recalling that $\nabla u u = \frac{1}{2}\nabla|u|^2$. Integrating by parts:

$$\rho^{\mathrm{f}} \int_\Omega \mathbf{u}_h^{n-1} \cdot \nabla \mathbf{u}_h^n \mathbf{u}_h^n = \rho^{\mathrm{f}} \int_\Omega \mathbf{u}_h^{n-1} \cdot \left(\frac{1}{2}\nabla|\mathbf{u}_h^n|^2 \right) = \frac{\rho^{\mathrm{f}}}{2} \left[\int_{\partial\Omega} \mathbf{u}_h^{n-1} \cdot \mathbf{n}|\mathbf{u}_h^n|^2 - \int_\Omega \nabla \cdot \mathbf{u}_h^{n-1}|\mathbf{u}_h^n|^2 \right]$$

Unlike the continuous case, the integral $\int_\Omega \nabla \cdot \mathbf{u}_h^{n-1}|\mathbf{u}_h^n|^2$ is not necessarily null: indeed we can not say that $\nabla \cdot \mathbf{u}_h^n = 0$ point-wisely in Ω. We only have that

$$\int_\Omega \nabla \cdot \mathbf{u}_h^n\, q = 0$$

In order to avoid this trouble, we can use Temam's trick by adding the term $\int_\Omega (\nabla \cdot \mathbf{u}_h^{n-1})\mathbf{u}_h^n\mathbf{u}_h^n$. This term is strongly consistent, because, when substituting the continuous solution $\mathbf{u}$ we would get $\nabla \cdot \mathbf{u} = 0$. Thus, obtaining:

$$\rho^{\mathrm{f}} \int_\Omega \mathbf{u}_h^{n-1} \cdot \nabla \mathbf{u}_h^n \mathbf{u}_h^n = \frac{\rho^{\mathrm{f}}}{2} \left[\int_{\partial\Omega} \mathbf{u}_h^{n-1} \cdot \mathbf{n}|\mathbf{u}_h^n|^2 - \int_\Omega \nabla \cdot \mathbf{u}_h^{n-1}|\mathbf{u}_h^n|^2 + \int_\Omega (\nabla \cdot \mathbf{u}_h^{n-1})\mathbf{u}_h^n\mathbf{u}_h^n \right]$$

$$= \frac{\rho^{\mathrm{f}}}{2} \sum_{i=1}^2 \int_{\Gamma_i^{\mathrm{out}}} \mathbf{u}_h^{n-1} \cdot \mathbf{n}|\mathbf{u}_h^n|^2$$

In such a way, the second and the third integral cancel out. Additionally, under the assumption $\mathbf{u}^n = 0$ on $\Gamma^{\mathrm{in}} \cup \Gamma^{\mathrm{wall}}$, the only terms that remain are the boundary ones on the outlets. For the

last term of (7), exploiting the definition of $\boldsymbol{\sigma}(\mathbf{u}^n, p^n)$:

$$\int_\Omega \nabla \cdot \boldsymbol{\sigma}(\mathbf{u}_h^n, p_h^n) \mathbf{u}_h^n = \int_{\partial\Omega} \boldsymbol{\sigma}(\mathbf{u}_h^n, p_h^n) \mathbf{n} \cdot \mathbf{u}_h^n - 2\mu \int_\Omega |\varepsilon(\mathbf{u}_h^n)|^2$$

Let us concentrate on the first term:

$$\int_{\partial\Omega} \boldsymbol{\sigma}(\mathbf{u}_h^n, p_h^n) \mathbf{n} \cdot \mathbf{u}_h^n = \sum_{i=1}^{2} \int_{\Gamma_i^{\text{out}}} \left(\frac{\rho^{\text{f}}}{2} |\mathbf{u}_h^{n-1} \cdot \mathbf{n}|_- \mathbf{u}_h^n - p_{\text{out},i,h}^n \mathbf{n} \right) \cdot \mathbf{u}_h^n$$

$$= \sum_{i=1}^{2} \left[\int_{\Gamma_i^{\text{out}}} \left(\frac{\rho^{\text{f}}}{2} |\mathbf{u}_h^{n-1} \cdot \mathbf{n}|_- |\mathbf{u}_h^n|^2 \right) - \int_{\Gamma_i^{\text{out}}} \left(p_d + R_{d,i} \int_{\Gamma_i^{\text{out}}} \mathbf{u}_h^{n-1} \cdot \mathbf{n} \right) \mathbf{n} \cdot \mathbf{u}_h^n \right]$$

$$= \sum_{i=1}^{2} \left[\int_{\Gamma_i^{\text{out}}} \left(\frac{\rho^{\text{f}}}{2} |\mathbf{u}_h^{n-1} \cdot \mathbf{n}|_- |\mathbf{u}_h^n|^2 \right) - \int_{\Gamma_i^{\text{out}}} p_d \mathbf{n} \cdot \mathbf{u}_h^n - R_{d,i} \int_{\Gamma_i^{\text{out}}} \left(\int_{\Gamma_i^{\text{out}}} \mathbf{u}_h^{n-1} \cdot \mathbf{n} \right) \mathbf{n} \cdot \mathbf{u}_h^n \right]$$

$$= \sum_{i=1}^{2} \left[\int_{\Gamma_i^{\text{out}}} \left(\frac{\rho^{\text{f}}}{2} |\mathbf{u}_h^{n-1} \cdot \mathbf{n}|_- |\mathbf{u}_h^n|^2 \right) - \int_{\Gamma_i^{\text{out}}} p_d \mathbf{n} \cdot \mathbf{u}_h^n - R_{d,i} \left(\int_{\Gamma_i^{\text{out}}} \mathbf{u}_h^{n-1} \cdot \mathbf{n} \right) \left(\int_{\Gamma_i^{\text{out}}} \mathbf{u}_h^n \cdot \mathbf{n} \right) \right]$$

Now, use the identity

$$R_{d,i} \left(\int_{\Gamma_i^{\text{out}}} \mathbf{u}^{n-1} \cdot \mathbf{n} \right) \left(\int_{\Gamma_i^{\text{out}}} \mathbf{u}^n \cdot \mathbf{n} \right) = R_{d,i} \left(\int_{\Gamma_i^{\text{out}}} (\mathbf{u}^{n-1} - \mathbf{u}^n) \cdot \mathbf{n} \right) \left(\int_{\Gamma_i^{\text{out}}} \mathbf{u}^n \cdot \mathbf{n} \right)$$

$$+ R_{d,i} \left| \int_{\Gamma_i^{\text{out}}} \mathbf{u}^n \cdot \mathbf{n} \right|^2$$

and apply Young's inequality to the first term of the identity to get:

$$\geq \sum_{i=1}^{2} \left[\int_{\Gamma_i^{\text{out}}} \left(\frac{\rho^{\text{f}}}{2} |\mathbf{u}_h^{n-1} \cdot \mathbf{n}|_- |\mathbf{u}_h^n|^2 \right) - \int_{\Gamma_i^{\text{out}}} p_d \mathbf{n} \cdot \mathbf{u}_h^n + \frac{R_{d,i}}{2} \left(\int_{\Gamma_i^{\text{out}}} (\mathbf{u}_h^n - \mathbf{u}_h^{n-1}) \cdot \mathbf{n} \right)^2 \right.$$

$$\left. + \frac{R_{d,i}}{2} \left(\int_{\Gamma_i^{\text{out}}} \mathbf{u}_h^n \cdot \mathbf{n} \right)^2 - R_{d,i} \left| \int_{\Gamma_i^{\text{out}}} \mathbf{u}_h^n \cdot \mathbf{n} \right|^2 \right]$$

Now, we can sum all the resulting terms together and notice that

$$\int_{\Gamma_i^{\text{out}}} \frac{\rho^{\text{f}}}{2} (\mathbf{u}_h^{n-1} \cdot \mathbf{n}) |\mathbf{u}_h^n|^2 - \int_{\Gamma_i^{\text{out}}} \frac{\rho^{\text{f}}}{2} |\mathbf{u}_h^{n-1} \cdot \mathbf{n}|_- |\mathbf{u}_h^n|^2 = \int_{\Gamma_i^{\text{out}}} \left(\frac{\rho^{\text{f}}}{2} |\mathbf{u}_h^{n-1} \cdot \mathbf{n}|_+ |\mathbf{u}_h^n|^2 \right)$$

where $|x|_+ = \max\{x, 0\}$. This is a positive quantity, that can be bounded from below by 0. In such case, it is possible to neglect it, creating an inequality. At the end, the remaining terms are:

$$\frac{\rho^{\text{f}}}{2\Delta t} \left[\|\mathbf{u}_h^n\|_{L^2(\Omega)}^2 - \|\mathbf{u}_h^{n-1}\|_{L^2(\Omega)}^2 + \|\mathbf{u}_h^n - \mathbf{u}_h^{n-1}\|_{L^2(\Omega)}^2 \right] + 2\mu \|\varepsilon(\mathbf{u}_h^n)\|_{L^2(\Omega)}^2$$

$$+ \sum_{i=1}^{2} \left[\int_{\Gamma_i^{\text{out}}} p_d \mathbf{n} \cdot \mathbf{u}_h^n - \frac{R_{d,i}}{2} \left(\int_{\Gamma_i^{\text{out}}} (\mathbf{u}_h^n - \mathbf{u}_h^{n-1}) \cdot \mathbf{n} \right)^2 + \frac{R_{d,i}}{2} \left(\int_{\Gamma_i^{\text{out}}} \mathbf{u}_h^n \cdot \mathbf{n} \right)^2 \right] \leq 0$$

8

Then we can bound the terms with the resistance to get

$$
\frac{\rho^{\mathrm{f}}}{2\Delta t}\left[\left\|\mathbf{u}_h^n\right\|_{L^2(\Omega)}^2 - \left\|\mathbf{u}_h^{n-1}\right\|_{L^2(\Omega)}^2 + \left\|\mathbf{u}_h^n - \mathbf{u}_h^{n-1}\right\|_{L^2(\Omega)}^2\right] + 2\mu\left\|\varepsilon(\mathbf{u}_h^n)\right\|_{L^2(\Omega)}^2 +
$$
$$
+ \sum_{i=1}^2\left[\int_{\Gamma_i^{\mathrm{out}}} p_d\mathbf{n}\cdot\mathbf{u}_h^n - \frac{R_{d,i}|\Gamma_i^{\mathrm{out}}|}{2}\left\|\mathbf{u}_h^n - \mathbf{u}_h^{n-1}\right\|_{L^2(\Gamma_i^{\mathrm{out}})}^2 + \frac{R_{d,i}|\Gamma_i^{\mathrm{out}}|}{2}\left\|\mathbf{u}_h^n\right\|_{L^2(\Gamma_i^{\mathrm{out}})}^2\right] \le 0
$$

Using the trace inequality:

$$
\|\mathbf{u}_h^n - \mathbf{u}_h^{n-1}\|_{L^2(\Gamma_i^{\mathrm{out}})}^2 \le C_T h^{-1}\|\mathbf{u}_h^n - \mathbf{u}_h^{n-1}\|_{L^2(\Omega)}^2
$$

We obtain:

$$
\frac{\rho^{\mathrm{f}}}{2\Delta t}\left[\left\|\mathbf{u}_h^n\right\|_{L^2(\Omega)}^2 - \left\|\mathbf{u}_h^{n-1}\right\|_{L^2(\Omega)}^2 + \left\|\mathbf{u}_h^n - \mathbf{u}_h^{n-1}\right\|_{L^2(\Omega)}^2\right] + 2\mu\left\|\varepsilon(\mathbf{u}_h^n)\right\|_{L^2(\Omega)}^2
$$
$$
+ \sum_{i=1}^2\left[\frac{R_{d,i}|\Gamma_i^{\mathrm{out}}|}{2}C_T h^{-1}\left\|\mathbf{u}_h^n\right\|_{L^2(\Omega)}^2 - \frac{R_{d,i}}{2}|\Gamma_i^{\mathrm{out}}|C_T h^{-1}\|\mathbf{u}_h^n - \mathbf{u}_h^{n-1}\|_{L^2(\Omega)}^2\right] \le 0
$$

The scheme is stable as long as all the coefficients are positive, hence for $\left\|\mathbf{u}^n - \mathbf{u}^{n-1}\right\|_{L^2(\Omega)}^2$:

$$
\frac{\rho^{\mathrm{f}}}{2\Delta t} - \sum_{i=1}^2 \frac{R_{d,i}}{2}|\Gamma_i^{\mathrm{out}}|C_T h^{-1} \ge 0 \qquad \Rightarrow \qquad \Delta t \le \frac{\rho^{\mathrm{f}}h}{C_T\sum_{i=1}^2 R_{d,i}|\Gamma_i^{\mathrm{out}}|}
$$

$\square$

Noting that the terms involving $\|\mathbf{u}_h^n - \mathbf{u}_h^{n-1}\|_{L^2(\Omega)}^2$ are now strictly positive, we can move them to the other side of the inequality and omit them. The final step in order to obtain an energy estimate is to multiply by Δt and $\sum_{m=1}^n$:

$$
\frac{\rho^{\mathrm{f}}}{2}\|\mathbf{u}_h^n\|_{L^2(\Omega)}^2 + 2\mu\Delta t\sum_{m=1}^n\|\varepsilon(\mathbf{u}_h^m)\|_{L^2(\Omega)}^2 + \sum_{m=1}^n\sum_{i=1}^2\frac{R_{d,i}|\Gamma_i^{\mathrm{out}}|}{2}C_T h^{-1}\Delta t\|\mathbf{u}_h^m\|_{L^2(\Omega)}^2 \le \frac{\rho^{\mathrm{f}}}{2}\left\|\mathbf{u}_h^0\right\|_{L^2(\Omega)}^2
$$

1.5   Alternative semi-discretization of the boundary condition

Consider an alternative semi-discretization on $\Gamma_i^{\mathrm{out}}, i = 1, 2$ given by

$$
\boldsymbol{\sigma}(\mathbf{u}^n, p^n)\mathbf{n} - \frac{\rho^{\mathrm{f}}}{2}|\mathbf{u}^{n-1}\cdot\mathbf{n}|_-\mathbf{u}^n + \frac{R_{d,i}|\Gamma_i^{\mathrm{out}}|}{2}(\mathbf{u}^n - \mathbf{u}^{n-1})\cdot\mathbf{n}\mathbf{n} = -p_{\mathrm{out},1}^n\mathbf{n} \quad\text{on } \Gamma_1^{\mathrm{out}} \qquad (8)
$$

The new added term introduces a difference in velocities $\mathbf{u}^n - \mathbf{u}^{n-1}$, which penalises abrupt changes in normal velocity across time steps: it smooths variations in the outflow velocity, preventing sudden fluctuations. The introduction of this additional term is consistent with $(3)_{3,4}$ because it is null when inserting the exact solution $\mathbf{u}$.

Regarding the energy estimate, following the same steps outlined in the proof of Lemma 1.1,

we achieve

$$
\frac{\rho^{\mathrm{f}}}{2\Delta t} \left[\left\| \mathbf{u}_h^n \right\|_{L^2(\Omega)}^2 - \left\| \mathbf{u}_h^{n-1} \right\|_{L^2(\Omega)}^2 + \left\| \mathbf{u}_h^n - \mathbf{u}_h^{n-1} \right\|_{L^2(\Omega)}^2 \right]
$$
$$
+ 2\mu \left\| \varepsilon(\mathbf{u}_h^n) \right\|_{L^2(\Omega)}^2 + \sum_{i=1}^{2} \left[\frac{R_{d,i} |\Gamma_i^{\mathrm{out}}|}{2} C_T h^{-1} \left\| \mathbf{u}_h^n \right\|_{L^2(\Omega)}^2 \right.
$$
$$
\left. - \frac{R_{d,i}}{2} |\Gamma_i^{\mathrm{out}}| C_T h^{-1} \|\mathbf{u}_h^n - \mathbf{u}_h^{n-1}\|_{L^2(\Omega)}^2 + \frac{R_{d,i}}{2} |\Gamma_i^{\mathrm{out}}| C_T h^{-1} \|\mathbf{u}_h^n - \mathbf{u}_h^{n-1}\|_{L^2(\Omega)}^2 \right] \leq 0
$$

As a result, the terms involving $\left\| \mathbf{u}_h^n - \mathbf{u}_h^{n-1} \right\|_{L^2(\Omega)}^2$ cancel out, leading to an energy stability estimate that is now unconditionally stable. This is because all the coefficients in the equation are positive, ensuring that the solution remains stable regardless of the time step size Δt.

1.6   Numerical implementation

The problems are implemented and tested using FreeFem++. In particular, the code includes the possibility of choosing any of the spaces presented in Section 1.3 (see [4] for the definition of the spaces in FreeFem++ framework). An example plot of the evolution of the velocity and of the pressure over a cycle with $(4)_{5,6}$ is shown in Figure 3. At the initial time, the velocity is relatively uniform. As time progress, the formation of more complex structures is visible, likely due to flow separation and shear layers forming at the bifurcation. For the pressure, initially, it presents a simple and clear color gradient. Then, the pressure distribution shows some pronounced regions of low and high pressure, indicating strong interactions between the flow streams.

It is important to note that this simulation was run with a sufficiently small time step. In fact, simply increasing Δt to 0.1 results in a highly unstable flow. This is in agreement with the theoretical predictions from Lemma 1.1: indeed, the finer the mesh, the smaller Δt has to be. FreeFem++ provides a very easy way of calculating the mesh size h, with the command `hTriangle.max` [4].

After a first visual inspection, it is relevant to study some meaningful quantities such as the average pressure on the inlet and the outlets, as well as the flux through those boundaries:

$$
\frac{1}{|\omega|} \int_\omega p_h^n, \qquad \int_\omega \mathbf{u}_h^n \cdot \mathbf{n} \qquad \omega \in \{\Gamma^{\mathrm{in}}, \Gamma_1^{\mathrm{out}}, \Gamma_2^{\mathrm{out}}\}
$$

The evolution of these quantities over time is illustrated in Figure 4. It is relevant to notice the periodicity of the results: both the flux and the average pressure are characterized by alternating phases of spikes and constant values. This directly reflects the periodic nature of the inlet function itself. A couple of remarks must be made on the flux plots. First, the inlet flux assumes negative values since we are considering the normal vector to be directed outwards, hence $\mathbf{u} \cdot \mathbf{n} < 0$. Secondly, we would expect to have mass conservation, meaning that all the fluid entering through the inlet must exit through the two outlets. Mathematically, this condition reads:

$$
\sum_{\omega \in \{\Gamma^{\mathrm{in}}, \Gamma_1^{\mathrm{out}}, \Gamma_2^{\mathrm{out}}\}} \int_\omega \mathbf{u}_h^n \cdot \mathbf{n} = 0
$$

Figure 4 shows that this balance is consistently maintained throughout the entire simulation, confirming the expected conservation of mass.
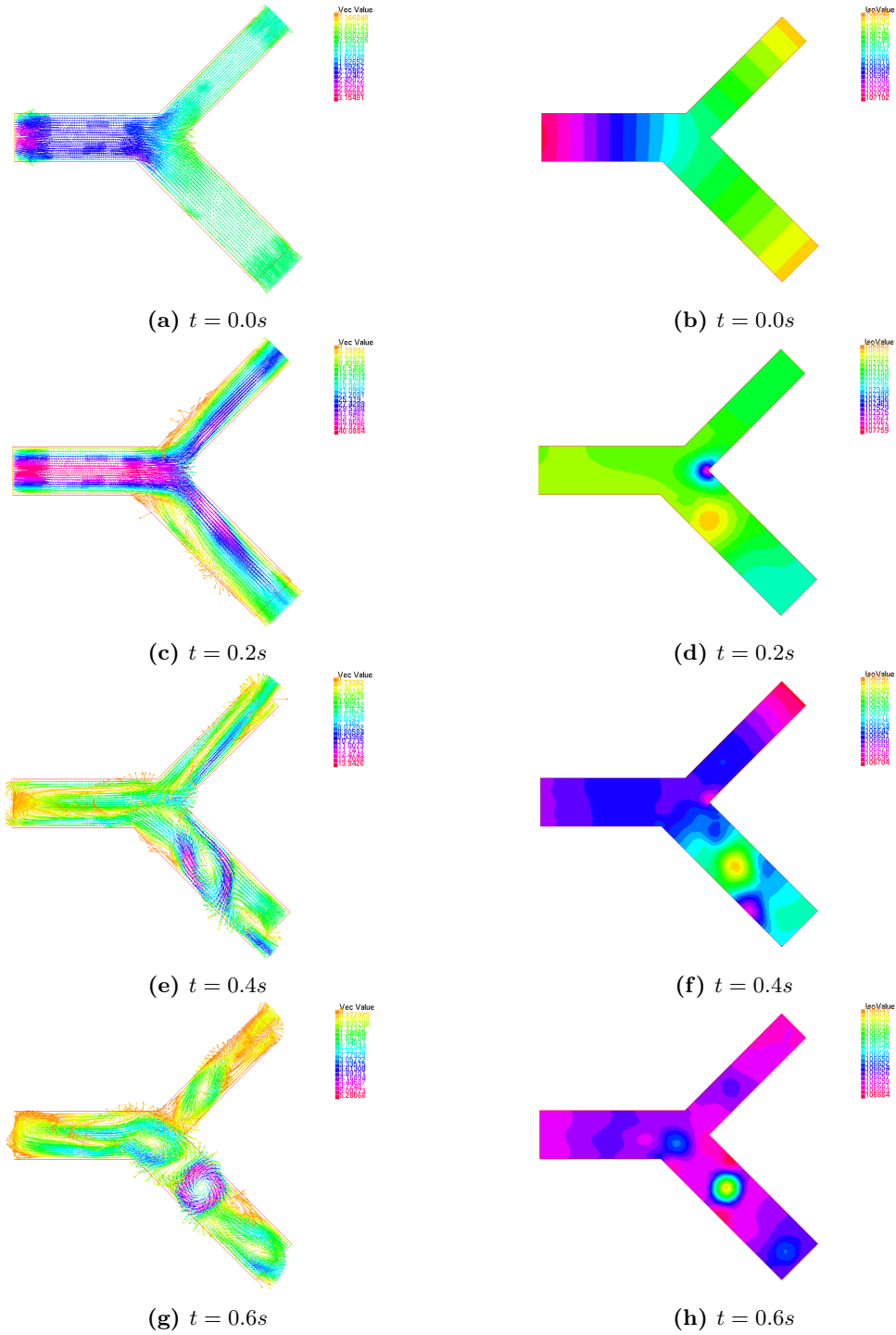
(a) $t = 0.0s$ **(b)** $t = 0.0s$

(c) $t = 0.2s$ **(d)** $t = 0.2s$

(e) $t = 0.4s$ **(f)** $t = 0.4s$

(g) $t = 0.6s$ **(h)** $t = 0.6s$

Figure 3: *Evolution of the velocity (on the left) and of the pressure (on the right) at different time instances ($\Delta t = 0.01$ and $h = 0.1096$), over the time span of one cycle, with $R_i = 100, i = 1, 2$, using $\mathbb{P}^2 - \mathbb{P}^1$ elements*

.

As well as the flux plot, also the pressure exhibits a periodic behavior. However, as $R_{d,i}$ increases, the outlet pressures tend to rise, which aligns with the expected effect of a higher

downstream resistance leading to increased backpressure. If $R_{d,i}$ is large, even small variations in flux would cause significant changes in the outlet pressure, implying that it is very sensitive to any fluctuation. Moreover, since a higher outlet pressure opposes flow reversal, the stabilizing effect becomes more pronounced. This could be seen in Figure 4. Indeed, in the simulations, when $R_{d,i} = 100$, the lower resistance allows the pressure to be less affected by flow fluctuations and remains closer to the initial value p_d. On the other hand, when $R_{d,i} = 800$ the higher resistance leads to a significantly higher outlet pressure, which opposes the reversal of flow.

Formulation with (8) boundary conditions has also been implemented. This formulation, contrary to the previous one, turned out to be stable for every time step Δt, as expected. It also provided consistent results, (Figure 4), proving the correctness of the implementation.
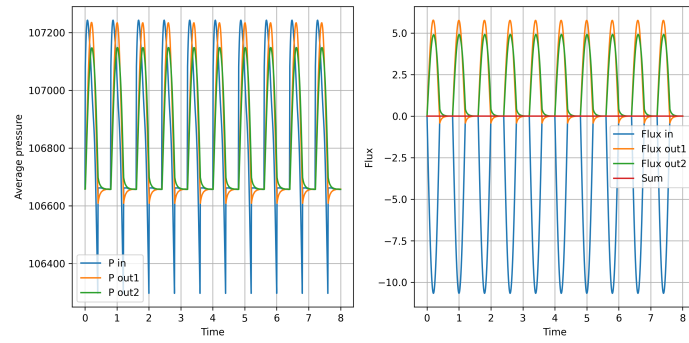
(a) $R_i = 100, i = 1, 2$
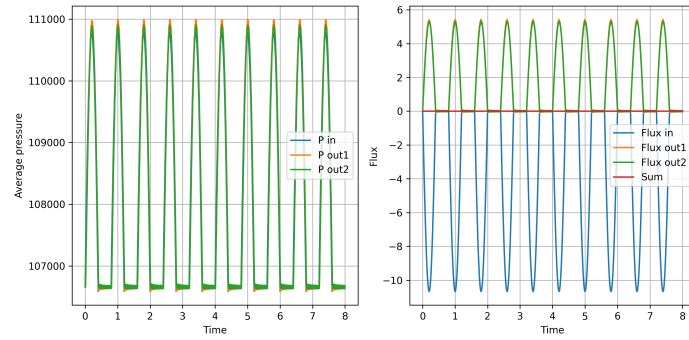
(b) $R_i = 800, i = 1, 2$
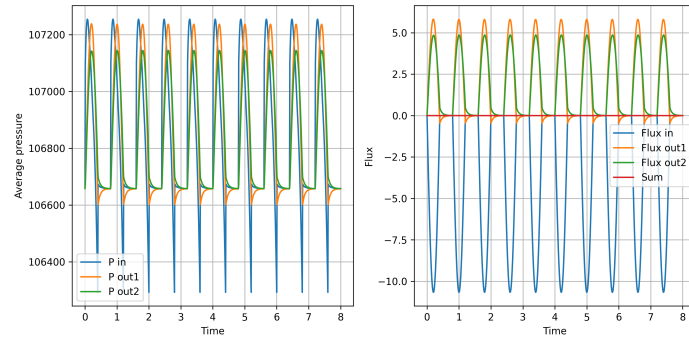
(c) $R_i = 100, i = 1, 2$, with alternative boundary condition

Figure 4: *Plot of the average pressure on the boundaries and of the flux through the boundaries, as well as the sum of all the fluxes, with respect to time (in seconds).*

2 Explicit Coupling and Added Mass in FSI

The second part of the project aims to analyze the instability issues arising when using explicit numerical schemes in fluid-structure interaction problems. In particular, we want to model the propagation of a wave in an elastic rectangular tube $\Omega = [0, L] \times [0, R]$ with $L = 6$ and $R = 0.5$ (Figure 5). The interface of the tube is denoted by Σ.
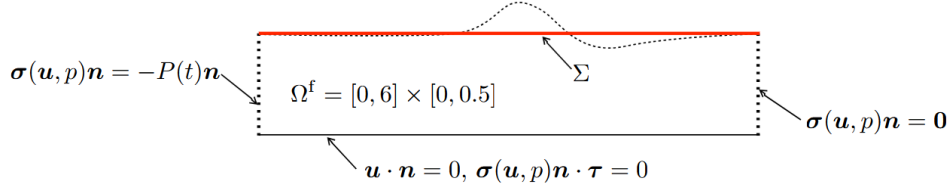
$$\boldsymbol{\sigma}(\boldsymbol{u}, p)\boldsymbol{n} = -P(t)\boldsymbol{n} \qquad \Sigma$$

$$\Omega^{\mathrm{f}} = [0, 6] \times [0, 0.5] \qquad \boldsymbol{\sigma}(\boldsymbol{u}, p)\boldsymbol{n} = \boldsymbol{0}$$

$$\boldsymbol{u} \cdot \boldsymbol{n} = 0, \ \boldsymbol{\sigma}(\boldsymbol{u}, p)\boldsymbol{n} \cdot \boldsymbol{\tau} = 0$$

Figure 5: *Computational domain Ω. The boundaries are numbered following an anticlockwise motion starting from the bottom.*

Given $T > 0$, we look for the velocity $\mathbf{u} : \Omega \times (0, T) \to \mathbb{R}^2$ and the pressure $p : \Omega \times (0, T) \to \mathbb{R}$, the vertical displacement of the solid $\eta : \Sigma \times (0, T) \to \mathbb{R}$ and the vertical velocity of the solid $\dot{\eta} : \Sigma \times (0, T) \to \mathbb{R}$ that solve

$$
\begin{cases}
\rho^{\mathrm{f}} \dfrac{\partial \mathbf{u}}{\partial t} - \nabla \cdot \boldsymbol{\sigma}(\mathbf{u}, p) = \mathbf{0} & \text{in } \Omega^{\mathrm{f}} \times (0, T), \\
\nabla \cdot \mathbf{u} = 0 & \text{in } \Omega^{\mathrm{f}} \times (0, T), \\
\mathbf{u} \cdot n = 0, \quad \boldsymbol{\sigma}(\mathbf{u}, p)\mathbf{n} \cdot \boldsymbol{\tau} = 0 & \text{on } \Gamma_1 \times (0, T), \\
\boldsymbol{\sigma}(\mathbf{u}, p)\mathbf{n} = -P\mathbf{n} & \text{on } \Gamma_2 \times (0, T), \\
\boldsymbol{\sigma}(\mathbf{u}, p)\mathbf{n} = \mathbf{0} & \text{on } \Gamma_4 \times (0, T),
\end{cases}
\tag{9}
$$

$$
\begin{cases}
\mathbf{u} \cdot \mathbf{n} = \dot{\eta}, \quad \mathbf{u} \cdot \boldsymbol{\tau} = \mathbf{0} & \text{on } \Sigma \times (0, T), \\
\rho^{\mathrm{s}} \epsilon \dfrac{\partial \dot{\eta}}{\partial t} - c_1 \dfrac{\partial^2 \eta}{\partial x^2} + c_0 \eta = -\boldsymbol{\sigma}(\mathbf{u}, p)\mathbf{n} \cdot \mathbf{n} & \text{on } \Sigma \times (0, T), \\
\dot{\eta} = \dfrac{\partial \eta}{\partial t} & \text{on } \Sigma \times (0, T), \\
\eta = 0 & \text{on } \partial\Sigma \times (0, T).
\end{cases}
\tag{10}
$$

with initial conditions $\mathbf{u}(0) = \mathbf{0}$, $\eta(0) = 0$ and $\dot{\eta}(0) = 0$. We recall the definition of $\boldsymbol{\sigma}(\mathbf{u}, p)$ and $\varepsilon(\mathbf{u})$ as in (2). To simplify the notation, from now on, define the operator $L^{\mathrm{s}} : H^2(\Sigma) \cap H_0^1(\Sigma) \to L^2(\Sigma)$ as

$$
L^{\mathrm{s}}\eta = -c_1 \frac{\partial^2 \eta}{\partial x^2} + c_0 \eta
$$

where c_1 and c_0 are the elastic parameter of the wall.

2.1 Semi-discrete schemes

We want to write the strong formulation of (9-10). As done in the previous section, given a time step Δt, time is discretized as $t_n = n\Delta t$ and the approximations at t_n are denoted by $\mathbf{u}^n$, p^n, η^n, $\dot{\eta}^n$. We use an implicit Euler scheme for the fluid and solid equations.

The strong formulation reads:

Given $\mathbf{u}_0 = \mathbf{u}(0)$, find $(\mathbf{u}^n, p^n)$ $\forall n \geq 1$ such that

$$
\begin{cases}
\rho^{\mathrm{f}} \dfrac{\mathbf{u}^n - \mathbf{u}^{n-1}}{\Delta t} - \nabla \cdot \boldsymbol{\sigma}(\mathbf{u}^n, p^n) = \mathbf{0} & \text{in } \Omega^{\mathrm{f}} \times (0, T) \\[2mm]
\nabla \cdot \mathbf{u}^{n+1} = 0 & \text{in } \Omega^{\mathrm{f}} \times (0, T) \\[2mm]
\mathbf{u}^n \cdot \mathbf{n} = 0, \quad \boldsymbol{\sigma}(\mathbf{u}^n, p^n)\mathbf{n} \cdot \boldsymbol{\tau} = 0 & \text{on } \Gamma_1 \times (0, T) \\[2mm]
\boldsymbol{\sigma}(\mathbf{u}^n, p^n)\mathbf{n} = -P^n \mathbf{n} & \text{on } \Gamma_2 \times (0, T) \\[2mm]
\boldsymbol{\sigma}(\mathbf{u}^n, p^n)\mathbf{n} = \mathbf{0} & \text{on } \Gamma_4 \times (0, T)
\end{cases}
$$

$$
\begin{cases}
\mathbf{u}^n \cdot \boldsymbol{\tau} = 0 & \text{on } \Sigma \\[2mm]
\rho^{\mathrm{s}} \epsilon \dfrac{\dot{\eta}^n - \dot{\eta}^{n-1}}{\Delta t} + L^{\mathrm{s}} \eta = -\boldsymbol{\sigma}(\mathbf{u}^n, p^n)\mathbf{n} \cdot \mathbf{n} & \text{on } \Sigma \times (0, T) \\[2mm]
\dot{\eta}^n = \dfrac{\eta^n - \eta^{n-1}}{\Delta t} & \text{on } \Sigma \times (0, T) \\[2mm]
\eta^n = 0 & \text{on } \partial\Sigma \times (0, T)
\end{cases}
$$

On the interface Σ, we consider three different schemes: fully implicit, and explicit with Dirichlet and Robin boundary conditions conditions. The coupling conditions read:

$$
\text{Implicit scheme:} \quad \mathbf{u}^n \cdot \mathbf{n} = \dot{\eta}^n \qquad\qquad\qquad\qquad\qquad \text{on } \Sigma \qquad (11)
$$

$$
\text{Explicit Dirichlet scheme:} \quad \mathbf{u}^n \cdot \mathbf{n} = \dot{\eta}^{n-1} \qquad\qquad\qquad\qquad \text{on } \Sigma \qquad (12)
$$

$$
\text{Explicit Robin scheme:} \quad \boldsymbol{\sigma}(\mathbf{u}^n, p^n)\mathbf{n} + \frac{\rho^{\mathrm{s}} \epsilon}{\Delta t} \mathbf{u}^n = \frac{\rho^{\mathrm{s}} \epsilon}{\Delta t} \dot{\eta}^{n-1} - L^{\mathrm{s}} \eta^{n-1} \qquad \text{on } \Sigma \qquad (13)
$$

The implicit scheme ensures a fully implicit coupling between the fluid and the structure. The normal velocity of the fluid matches the velocity of the interface at the same time step n, enforcing a strong two-way interaction. The explicit Dirichlet scheme evaluates $\dot{\eta}$ at the previous step, which uncouples the system. As we will see later, this choice is affected by numerical instability under certain choices of the physical parameters. Lastly, the explicit Robin [5] is a specific case of a more general equation (see [6] with $\alpha = \rho^{\mathrm{s}} \epsilon / \Delta t$). The explicit treatment of the elastic term $L^{\mathrm{s}} \eta^{n-1}$ enables a natural splitting. Robin's coupling condition is particularly useful in mitigating the added mass effect, which can lead to numerical instabilities when the density of the structure is close to that of the fluid. The Robin condition alleviates this issue by incorporating part of the solid's inertial effects and guaranteeing added-mass free stability.

When neglecting viscosity, i.e. $\mu = 0$, and considering that the system is isolated, i.e. $p = 0$ on $\Gamma_2 \cup \Gamma_4$, each of the three problems resulting from the three coupling conditions (11)-(12)-(13) can be easily manipulated into a 1D equation using the added-mass operator $\mathcal{M}_a : H^{-1/2}(\Sigma) \to H^{1/2}(\Sigma)$. This is a local operator such that

$$
\mathcal{M}_a g = q|_\Sigma \quad \text{where } q \in H^1(\Omega^{\mathrm{f}}) \text{ solves} \quad
\begin{cases}
-\Delta q = 0 & \text{in } \Omega^{\mathrm{f}} \\[1mm]
q = 0 & \text{on } \Gamma_2 \cup \Gamma_4 \\[1mm]
\dfrac{\partial q}{\partial n} = 0 & \text{on } \Gamma_1 \\[1mm]
\dfrac{\partial q}{\partial n} = g & \text{on } \Sigma
\end{cases}
$$

Thus the equations we obtain are:

$$\text{Implicit scheme:} \quad \rho^{\text{s}}\epsilon\,\partial_t\dot{\eta}^n + \rho^{\text{f}}\mathcal{M}_a\partial_t\dot{\eta}^n + L^{\text{s}}\eta^n = 0$$

$$\text{Explicit Dirichlet scheme:} \quad \rho^{\text{s}}\epsilon\,\partial_t\dot{\eta}^n + \rho^{\text{f}}\mathcal{M}_a\partial_t\dot{\eta}^{n-1} + L^{\text{s}}\eta^n = 0$$

$$\text{Explicit Robin scheme:} \quad \rho^{\text{s}}\epsilon\,\partial_t\dot{\eta}^n + \rho^{\text{f}}\mathcal{M}_a\partial_t\dot{\eta}^{n-1} + \frac{\Delta t}{\epsilon\rho^{\text{s}}}\mathcal{M}_a L^{\text{s}}\dot{\eta}^{n-1} + L^{\text{s}}\eta^n = 0$$

The purpose of the next sections is to study the numerical stability of the three proposed methods using FreeFem++ framework. The problems are simulated for a computational time $T = 1.5 \times 10^{-2}$. A sinusoidal pressure wave of amplitude $P_{\max} = 2 \cdot 10^4$, is prescribed on the boundary Γ_4 for a duration equal to half of the period. On Γ_2, we set a null pressure, and a slip condition is imposed on Γ_1. The solid is fixed with $\eta = 0$ on the lateral boundaries.

2.2 Numerical stability of the explicit Dirichlet scheme

Each of the approaches presented earlier has some advantages and some drawbacks. For instance, the explicit Dirichlet scheme is suitable to solve a fully uncoupled problem. Unlike the implicit method, where both systems must be solved simultaneously by assigning one boundary condition to each system, the explicit scheme allows us to solve the fluid and structure equations separately. This reduces the computational complexity and facilitates the use of independent solvers. On the other hand, this scheme comes with a major drawback: its numerical stability is dictated by the problem variables. The scheme is unconditionally unstable when

$$\frac{\rho^{\text{f}}\alpha_{\max}}{\rho^{\text{s}}\epsilon} > 1 + \frac{C_0\Delta t^2}{4\rho^{\text{s}}\epsilon} \tag{14}$$

where $\alpha_{\max} = \max_{n\in\mathbb{N}}\{\alpha_n\}$ is the largest eigenvalue of $\mathcal{M}_a$ that depends on physical parameters. Since Δt is supposed to be small enough, in order to correctly capture the evolution, we can simplify (14) as

$$\frac{\rho^{\text{f}}\alpha_{\max}}{\rho^{\text{s}}\epsilon} > 1, \qquad \alpha_{\max} \approx \frac{L^2}{\pi^2 R} \tag{15}$$

Running the `fsi-DN.edp` code, without modifying any parameters, reveals that the explicit Dirichlet scheme is highly unstable, causing the elastic tube to undergo significant oscillations in less than a millisecond (Figure 6). This occurs because condition (15) is being satisfied: considering $\epsilon = 0.1$, $L = 6$, $R = 0.5$, $\rho^{\text{f}} = 1.0$ and $\rho^{\text{s}} = 1.1$, we obtain

$$\frac{\rho^{\text{f}}\alpha_{\max}}{\rho^{\text{s}}\epsilon} = 66.38 \gg 1$$

Since this condition does not depend on the time step Δt, adjusting its value will not improve numerical stability. Indeed, running the same code for a lower value of Δt will produce the same identical results. The only way to resolve the issue would be to either increase the solid density or decrease the fluid density, which would fundamentally alter the physics of the problem. Figure 7 shows a numerical simulation with a suitable value of ρ^{f}. The solution no longer exhibits strong oscillations as before. Instead, the top boundary undergoes deformation, initially forming undulations that propagate along its length. Over time, these waves smooth out and decrease in amplitude. A greater difference between the two densities results in a smaller initial bump.
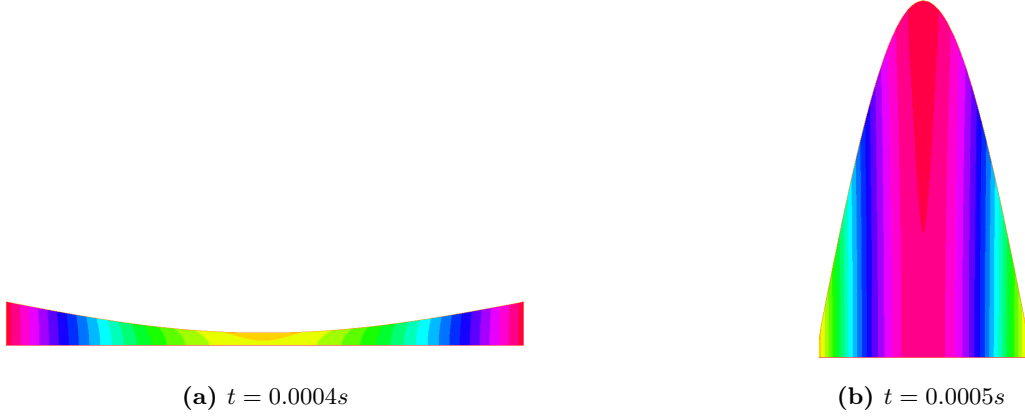
(a) $t = 0.0004s$ **(b)** $t = 0.0005s$

Figure 6: *Plot of the pressure in Ω at two different time instances, showing the instability of the explicit Dirichlet scheme with $\rho^f = 1.0$ and $\rho^s = 1.1..$*

(a) $t = 0.001s$

(b) $t = 0.003s$

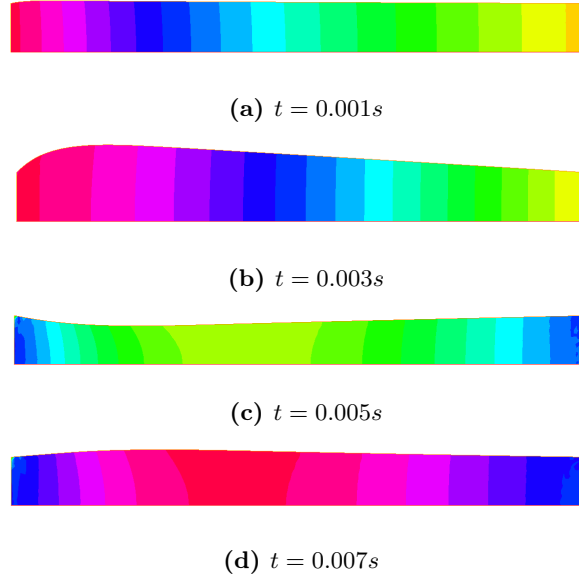
(c) $t = 0.005s$

(d) $t = 0.007s$

Figure 7: *Plot of the pressure in Ω at different time instances, showing the stability of the explicit Dirichlet scheme with $\rho^f = 0.005$ and $\rho^s = 1.1$.*

2.3   Numerical stability of the explicit Robin scheme

The results (Figure 8), obtained simply running `fsi-RN.edp`, indicate a numerically stable approximation: the solution does not exhibit any unphysical oscillations or numerical instabilities. Choosing the same values as in the simulation show in Figure 7, we obtain the same behavior, showing coherence and correctness of the two methods.

As found in [6], the value of the Robin parameter $\alpha = \rho^s \epsilon / \Delta t$ should be between 250 and 2000 to guarantee the best accuracy of the solution. Further discussion on the influence of the Robin parameter is done in [7]. In our case, considering $\rho^s = 1.1$, $\epsilon = 0.1$ and $\Delta t = 10^{-4}$, we obtain $\alpha = 1100$, which perfectly falls within the requested range.

Further studies are centered on demonstrating the need of introducing a Robin-type coupling
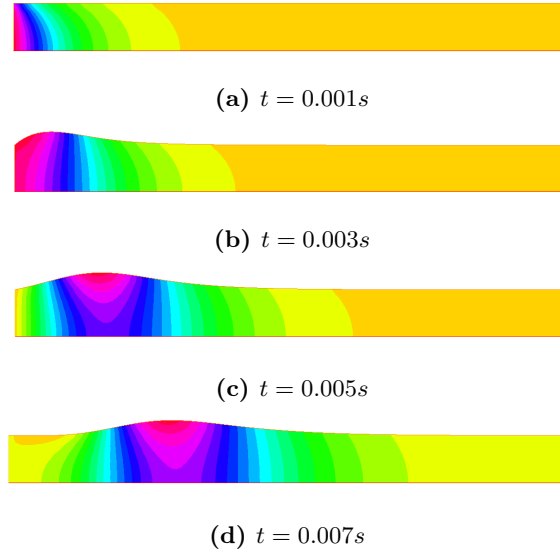
(a) $t = 0.001s$

(b) $t = 0.003s$

(c) $t = 0.005s$

(d) $t = 0.007s$

Figure 8: *Plot of the pressure in Ω at different time instances, showing the stability of the explicit Robin scheme with $\rho^f = 1.0$ and $\rho^s = 1.1$.*

condition. This method shows robustness with respect to the added mass effect. When a body moves in a fluid, it generates disturbances in the velocity field, causing pressure variations. These variations contribute to an additional force on the body, which can be interpreted as a virtual extra mass that the body must carry along with it in the fluid. This added mass depends on the body's geometry and the properties of the fluid: in particular, a high density ratio ρ^f/ρ^s and a thin and lengthy geometry could cause a greater added-mass. Therefore, we want to study the influence of variations in the density ratio and length of the domain L.

ρ^f	ρ^s	ρ^f/ρ^s	L
1.0	1.1	0.91	2
1.0	1.1	0.91	4
1.0	1.1	0.91	6
1.0	1.1	0.91	10
1.0	1.1	0.91	50

Table 1: *Simulations with varying domain length.*

ρ^f	ρ^s	ρ^f/ρ^s	L
1.0	1.1	0.91	6
2.2	1.1	2	6
10	1.1	≈ 10	6
100	1.1	≈ 100	6
0.1	1.1	≈ 0.1	6
0.01	1.1	≈ 0.01	6

Table 2: *Simulations with varying fluid density.*

To investigate this phenomenon, we firstly conducted simulations for different domain lengths L. The lengths considered are listed in Table 1, while the densities were kept constant at $\rho^f = 1.0$ and $\rho^s = 1.1$ across all simulations. When the domain length L is not sufficiently long, the generated wave propagates but eventually reflects back, affecting the dynamics of the system and preventing the wave to fully develop.

The same analysis was done changing the densities values while keeping the domain length to a fixed value, chosen to be $L = 6$. Table 2 summarizes the chosen values, with the respective ratio. When the fluid is significantly denser than the solid, the generated wave has a very low amplitude and propagates slowly. This is due to the fact that the fluid has a larger inertia,
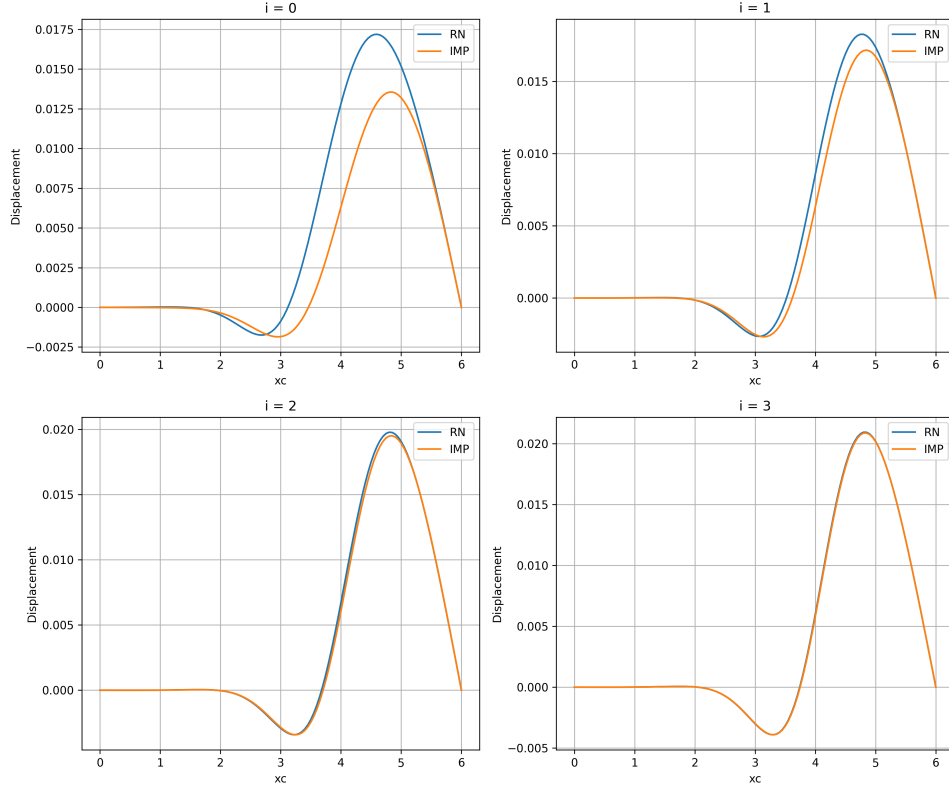
Figure 9: *Vertical displacement using the explicit Robin scheme and the implicit scheme at final time (t = 0.015s), for different values of i in ([2.4](#)), with $\rho^f = 1.0$, $\rho^s = 1.1$ and $L = 6$.*

making it less responsive to perturbations. On the other hand, when the density ratio is low, the wave is both bigger and faster. This can be attributed to the reduced inertia of the fluid, which allows the wave to develop more prominently and travel at a higher velocity.

In any case, no change in the parameter values affects the overall stability of the system. Despite variations in domain length and density ratio, the system remains stable throughout all simulations, indicating strong robustness of the method.

2.4 Comparison between explicit Robin and implicit scheme on displacement approximation

This last section aims to analyze the precision of the explicit Robin scheme, using 1st order extrapolation, compared to the implicit one. To carry out this study, the vertical displacement η is plotted along the top boundary in Figure [9](#). This is done for different values of Δt. We considered:

$$\Delta t = \frac{2 \cdot 10^{-4}}{2^i} \quad \text{with} \quad i = 0, 1, 2, 3$$

It is noticeable that the explicit Robin scheme converges to the solution provided by the implicit method while remaining stable. This behavior is in line with theoretical expectations. The same does not happen when we use a 0 order extrapolation, as previously demonstrated in [5]. It was also shown that the explicit Robin scheme is independent of the mesh size h [5].

These results highlight the potential of the explicit Robin scheme as a computationally ef-

ficient alternative to implicit methods, particularly in time-dependent problems where avoiding a fully implicit formulation can reduce computational costs. However, they also emphasize the importance of using first-order extrapolation, as lower-order approximations fail to ensure the same level of accuracy and stability.

3   Conclusions

In this work, we have investigated the numerical modeling of blood flow in a bifurcation and the stability of explicit schemes in fluid-structure interaction problems.

In the first part, we analyzed the Navier-Stokes equations for incompressible flows in a simplified arterial bifurcation. Through a variational formulation and numerical discretization in FreeFem++, we examined the role of different boundary conditions, ensuring conditional stability in the energy norm. Our results confirm that mass conservation is maintained throughout the simulation and that the pressure distribution correctly reflects the effects of downstream resistance.

In the second part, we explored explicit coupling schemes in FSI, highlighting the challenges posed by the added mass effect. The explicit Dirichlet scheme demonstrated severe numerical instabilities when the fluid and solid densities were similar, confirming theoretical predictions. In contrast, the explicit Robin scheme showed strong robustness, remaining stable across various configurations and density ratios, as well as being accurate in predicting the solid displacement.

References

[1] G. Arbia, I. Vignon-Clementel, T. Y. Hsia, and J. F. Gerbeau. Modified Navier-Stokes equations for the outflow boundary conditions in hemodynamics. *European Journal of Mechanics*, 60:175–188, 2016.

[2] Y. Bazilevs, J. R. Gohean, T. J. R. Hughes, R. D. Moser, and Y. Zhang. Patient-specific isogeometric Fluid-Structure Interaction analysis of thoracic aortic blood flow due to implantation of the Jarvik 2000 left ventricular assist device. *Institute for Computational Engineering and Sciences, The University of Texas at Austin*, 2000.

[3] A. Quarteroni. *Numerical Models for Differential Problems*. Springer, 2018.

[4] FreeFEM Development Team. *FreeFEM Documentation*, 2025.

[5] Miguel Angel Fernández, Jimmy Mullaert, and Marina Vidrascu. Explicit Robin-Neumann schemes for the coupling of incompressible fluids with thin-walled structures. *Computer Methods in Applied Mechanics and Engineering*, 267:566–593, 2013.

[6] E. Burman, R. Durst, M. A. Fernández, and J. Guzmán. Fully discrete loosely coupled Robin-Robin scheme for incompressible fluid-structure interaction: stability and error analysis. *Numerische Mathematik*, 151:807–840, 2022.

[7] G. Gigante and C. Vergara. On the stability of a loosely-coupled scheme based on a Robin interface condition for fluid-structure interaction. *Computers and Mathematics with Applications*, 96:109–119, 2021.